



Analysis of Tank PMD Rewetting Following Thrust Resettling

M.M. Weislogel and M.A. Sala
Portland State University, Portland, Oregon

S.H. Collicott
Purdue University, West Lafayette, Indiana

The NASA STI Program Office . . . in Profile

Since its founding, NASA has been dedicated to the advancement of aeronautics and space science. The NASA Scientific and Technical Information (STI) Program Office plays a key part in helping NASA maintain this important role.

The NASA STI Program Office is operated by Langley Research Center, the Lead Center for NASA's scientific and technical information. The NASA STI Program Office provides access to the NASA STI Database, the largest collection of aeronautical and space science STI in the world. The Program Office is also NASA's institutional mechanism for disseminating the results of its research and development activities. These results are published by NASA in the NASA STI Report Series, which includes the following report types:

- **TECHNICAL PUBLICATION.** Reports of completed research or a major significant phase of research that present the results of NASA programs and include extensive data or theoretical analysis. Includes compilations of significant scientific and technical data and information deemed to be of continuing reference value. NASA's counterpart of peer-reviewed formal professional papers but has less stringent limitations on manuscript length and extent of graphic presentations.
- **TECHNICAL MEMORANDUM.** Scientific and technical findings that are preliminary or of specialized interest, e.g., quick release reports, working papers, and bibliographies that contain minimal annotation. Does not contain extensive analysis.
- **CONTRACTOR REPORT.** Scientific and technical findings by NASA-sponsored contractors and grantees.

- **CONFERENCE PUBLICATION.** Collected papers from scientific and technical conferences, symposia, seminars, or other meetings sponsored or cosponsored by NASA.
- **SPECIAL PUBLICATION.** Scientific, technical, or historical information from NASA programs, projects, and missions, often concerned with subjects having substantial public interest.
- **TECHNICAL TRANSLATION.** English-language translations of foreign scientific and technical material pertinent to NASA's mission.

Specialized services that complement the STI Program Office's diverse offerings include creating custom thesauri, building customized databases, organizing and publishing research results . . . even providing videos.

For more information about the NASA STI Program Office, see the following:

- Access the NASA STI Program Home Page at <http://www.sti.nasa.gov>
- E-mail your question via the Internet to help@sti.nasa.gov
- Fax your question to the NASA Access Help Desk at 301-621-0134
- Telephone the NASA Access Help Desk at 301-621-0390
- Write to:
NASA Access Help Desk
NASA Center for AeroSpace Information
7121 Standard Drive
Hanover, MD 21076

NASA/CR—2002-211974



Analysis of Tank PMD Rewetting Following Thrust Resettling

M.M. Weislogel and M.A. Sala
Portland State University, Portland, Oregon

S.H. Collicott
Purdue University, West Lafayette, Indiana

Prepared under Contract NAS3-00126

National Aeronautics and
Space Administration

Glenn Research Center

October 2002

Acknowledgments

The authors would like to thank D. Chato, NASA Glenn Research Center, for helpful information concerning VTRE and for providing copies of VTRE flight video. We would also like to thank R. Finn for valuable insights. This work is supported in part through NASA's Microgravity Science and Applications Division through contract NAS3-00126 monitored by E. Ramé.

Available from

NASA Center for Aerospace Information
7121 Standard Drive
Hanover, MD 21076

National Technical Information Service
5285 Port Royal Road
Springfield, VA 22100

Available electronically at <http://gltrs.grc.nasa.gov>

ANALYSIS OF TANK PMD REWETTING FOLLOWING THRUST RESETTLING

M.M. Weislogel and M.A. Sala
Portland State University
Portland, Oregon 97207-0751

S.H. Collicott
Purdue University
West Lafayette, Indiana 47907-1968

Abstract

Recent investigations have successfully demonstrated closed-form analytical solutions of spontaneous capillary flows in idealized cylindrical containers with interior corners. In this report, the theory is extended and applied to complex containers modeling spacecraft fuel tanks employing propellant management devices (PMDs). The specific problem investigated is one of spontaneous rewetting of a typical partially filled liquid fuel/cryogen tank with PMD after thrust resettling. The transients of this flow impact the logistics of orbital maneuvers and potentially tank thermal control. The general procedure to compute the initial condition (mean radius of curvature for the interface) for the closed-form transient flows is first outlined then solved for several 'complex' cylindrical tanks exhibiting symmetry. The utility and limitations of the technique as a design tool are discussed in a summary, which also highlights comparisons with NASA flight data of a model propellant tank with PMD.

Introduction

Recent investigations have successfully demonstrated asymptotic techniques for the solution of spontaneous capillary flows in idealized containers with interior corners¹. The approach yields simple closed-form solutions for important features of the flow such as transient flow rate and 3-D interface shape without applying approximations such as hydraulic diameter, friction factors, or weighted capillary pressures. More recently, these techniques have

been applied to cylindrical containers of irregular polygonal cross-section², the results of which compare favorably with benchmark drop tower experiments.

In this report, the theory is further extended to complex containers modeling spacecraft fuel tanks employing propellant management devices (PMDs). However, the general approach is expected to be useful to many low-gravity fluids management and handling operations. The specific problem investigated is one of spontaneous rewetting of a typical partially filled liquid fuel tank with PMD after thrust resettling. The transients of this flow impact the logistics of orbital maneuvers and potentially tank thermal control, particularly when the liquid inventory represents a significant percentage of the total mass of the spacecraft.

The method of solution is briefly outlined where it is shown that the mean radius of curvature of the interface at equilibrium can be used to compute the pivotal initial condition for the flow throughout the container. This mean radius R may be expressed analytically for an important though restrictive class of simple containers using the approach of de Lazzer et al.³ It is shown herein that this approach may be extended to certain more complex containers that are symmetric. (Computations of R using *Surface Evolver*⁴ may be employed for containers of arbitrary complexity.) Once R is known, the existing analytical solutions may be applied and the key characteristics of the flow may be determined in closed form. Examples of tanks with central radial and radial wall vane PMDs are provided. Transient flow rates are presented

modeling the thrust resettling problem for three ‘complex’ containers patterned after the tank and PMD employed in the Vented Tank Resupply Experiment (VTRE Shuttle Flight Experiment). Despite the violation of several theoretical assumptions the results of comparisons to the VTRE data argue favorably for the use of the all-analytical approach as an efficient and accurate design tool to predict complex capillary flows in low-g propellant management systems. It is recommended that the approach also serve as a guide to fully transient 3-D numerical calculations (CFD).

Review of Flow in j th Corner

Detailed comparisons between experiments and theory have demonstrated that spontaneous capillary flows in irregular polygonal containers with j interior corners satisfying the Concus-Finn corner⁵ wetting condition are controlled by the local capillary flow in the corners². Assuming a wetting fluid and locally parallel flow $[(H_j/L)^2 \ll 1]$, the dimensionless leading order governing equations simplify to the nonlinear lubrication equation

$$h_t = 2h_z^2 + hh_{zz}, \quad (1)$$

where $h = h_j$ is the dimensionless height of the meniscus measured along the bisector of the j th corner at location z (see Fig. 1 for notation).

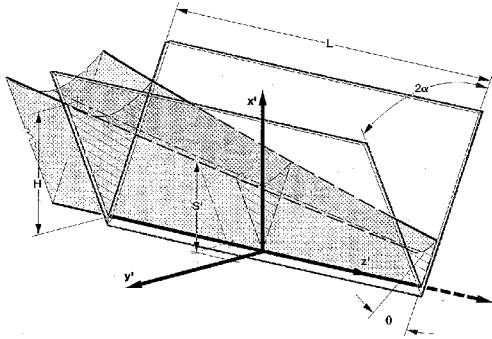


Figure 1. Fluid column in an isolated corner j , angle 2α . The 3-D surface profile is $S(y,z,t)$ with characteristic height and length, $H = H_j$ and $L = L_j$, respectively.

This implies that the capillary surface is a construct of circular arcs in the cross-flow plane (x - y plane), and, once $h(z,t)$ is determined, the entire 3-D transient surface is known from

$$S_j = h_j (1 + f_j) + (h_j^2 f_j^2 - y_j^2)^{1/2}, \quad (2)$$

where

$$|y_j| \leq h_j f_j \sin \delta_j,$$

and $\delta_j \equiv \pi/2 - \alpha_j - \theta$. The parameter f_j is the measure of interface curvature (driving force) in the j th corner satisfying the Concus-Finn condition ($\theta < \pi/2 - \alpha_j$) and is given by

$$f_j = \frac{\sin \alpha_j}{\cos \theta - \sin \alpha_j} \quad (3)$$

where θ is the contact angle and α_j is the particular corner half-angle. The static contact angle boundary condition is correct to leading order because the predominant flow direction is *parallel* to the contact line. The problem of sudden capillary rise^{6,7,1} (i.e. imbibition), akin to termination of thruster firing during routine tank settling, applies constraints $h(0,t) = 1$, $h(L,t) = 0$, and conservation of mass to eq. (1). The solution for the j th interior corner provides important design quantities such as liquid column length L_j , flow rate \dot{Q}_j , and position of the receding bulk meniscus z_b as functions of time. These quantities are provided below in *dimensional* form:

$$L_j = 1.702 G_j^{1/2} H_j^{1/2} t^{1/2} \quad (4)$$

$$\dot{Q}_j = 0.349 f_j^2 F_{Anj} G_j^{1/2} H_j^{5/2} t^{-1/2}, \quad (5)$$

where H_j is the constant height (a.k.a. constant pressure or curvature) condition at $z = 0$. The total flow rate may be determined simply as

$$\dot{Q}_{tot} = \sum_j \dot{Q}_j$$

and the location of the receding bulk meniscus is approximated² by

$$z_b = 1.702 \bar{\eta}_{br}^+ \left(\frac{R \sigma}{\mu} t \right)^{1/2} \quad (6)$$

where

$$\bar{\eta}_{br}^+ \approx \frac{-0.4103 \sum_{j=1}^n F_{Anj} F_{ij}^{1/2} (\cos \theta - \sin \alpha_j)}{\frac{A_n}{R^2} - \sum_{j=1}^n F_{Anj}}.$$

The geometric function

$$F_{Anj} = \frac{\cos \theta \sin \delta_j}{\sin \alpha_j} - \delta_j, \quad (7)$$

and G_j is given by

$$G_j = \frac{\sigma F_i \sin^2 \alpha_j}{\mu f_j}, \quad (8)$$

where F_i is a weak function of θ and α and may be treated as a constant $F_i \approx 0.142$ (see reference 1, Fig. 6 for exact value). Note also that $F_{ij} = (F_i)_j \approx 0.142$. σ and μ are the fluid surface tension and dynamic viscosity, respectively.

From eqs. (4) through (8) low gravity containers may be sized, fluids selected, or flow times predicted. Such quantities, which can be rapidly computed by hand, are accurate to $\pm 6\%$ for perfectly wetting fluids^{6,7,1} and represent an improvement over previous design relationships that used corner friction factors and weighted capillary pressures⁸.

However, the transients of the spontaneous corner flows may not be calculated without knowledge of H_j . The constant height H_j at $z = 0$ is directly related to the mean radius of curvature R of the interface at equilibrium for the container in question, which is a function of container size, shape, fill level, and liquid contact angle(s). R could also depend on the fluid's history if more than one local equilibrium interface configuration is possible. ($R \equiv 1/2\mathcal{H}$, where \mathcal{H} is the mean curvature of the interface.) For an important class of cylindrical containers with sufficiently planar interior corners satisfying the Concus-Finn condition

$$R = f_j H_j. \quad (9)$$

It is therefore necessary to determine R for the container before H_j and the subsequent transient flows in each corner may be computed.

Calculation of Tank Mean Radius of Curvature

In the zero-gravity environment, for cylindrical containers of arbitrary cross-section that possess at least one interior corner satisfying the Concus-Finn condition, de Lazzer et al.³ apply the divergence theorem to the Young-Laplace-Gauss equation

$$\nabla \cdot \frac{\nabla u}{\sqrt{1+|\nabla u|^2}} = \frac{1}{R}$$

over a presumed solution domain Ω^* bounded in part by circular arcs of radius R that cut off corner flow sections and meet the rigid walls in

the prescribed contact angle θ . See Figure 2 for the case of a rhombus. When such a domain can be found, the divergence theorem yields

$$\oint_{\Sigma_1 \cup \Sigma_2} \cos \theta^* ds = |\Omega^*|/R. \quad (10)$$

Here Σ_1 denotes the totality of boundary arcs on the rigid part of the boundary, and Σ_2 denotes the circular arcs that appear, see Figure 2b. On Σ_1 , $\theta^* = \theta$ is the prescribed contact angle of the liquid with the material of the containing vessel; in accordance with the method, θ^* is set equal to zero on Σ_2 , corresponding to the hypothesis that the fluid rises vertically on the Σ_2 arcs.

For the cases of regular polygonal and rhombic cylinders, de Lazzer et al found that by inserting arcs symmetrically into corners as indicated in Figure 2, a unique value of R consistent with the construction could be found. We outline that procedure for the rhombic case in eqs. (11) to (13) below. It does not follow directly from the method that the value thus determined actually corresponds to a solution of the form desired; however the correctness of the procedure for the case of a regular polygon was later demonstrated by Finn and Neel¹⁰. These authors go on to point out that in a general configuration the application of the method becomes difficult and additionally can lead to erroneous results. Nevertheless, the procedure does lead to formally solvable closed form expressions for R for a variety of relevant container section types, several of which have been verified experimentally: squares^{1,6}, rhombi⁷, rectangles¹, equilateral triangles¹, irregular triangles², and simple cylinders with regular vanes⁹. Although the hazards pointed out by Finn and Neel are real, one may presume on the basis of their success with the regular polygon that at least some of these special cases correctly represent reality. Beyond that, the close correlation we have found in the cases we consider, with numerical results from the *Surface Evolver* and comparison with experiment, speak strongly for the underlying correctness of the present application.

In a general case and especially for asymmetric configurations, strong caution must be advised. In the present paper, symmetric interfaces in symmetric containers will be assumed in like manner as in de Lazzer et al, since such interfaces are frequently observed in practice.

As illustrated in Fig. 2, for a cylinder with rhombic section where the Concus-Finn condition is only satisfied in the corners with acute angles³, along the i th portion of the perimeter the contact angle for use in eq. (10) is θ_i . The area contained within the projected perimeter is Ω^* and is identified by a heavier line weight in this and figures to follow. The sought mean radius of curvature of the interface is R . The dashed lines sketched in Fig. 2b will be discussed shortly.

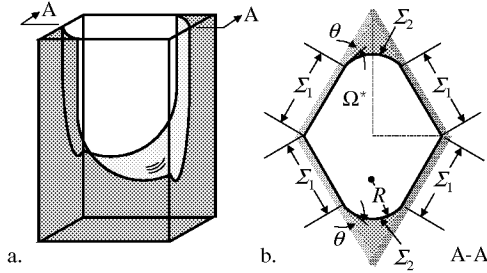


Figure 2. Rhombic cylinder with wetting of acute edges only, after de Lazzer et al³.

The left hand side of eq. (10) may be evaluated and represented as the summation of projected, interface perimeter lengths Σ_i , weighted by $\cos \theta_i$, and enclosing area Ω^* :

$$\sum_{i=1}^n \Sigma_i \cos \theta_i = |\Omega^*|/R. \quad (11)$$

For the polygonal section depicted in Fig. 2, $\theta_1 = \theta$, following de Lazzer et al $\theta_2 = 0$, and eq. (11) becomes

$$|\Sigma_1| \cos \theta + |\Sigma_2| = |\Omega^*|/R, \quad (12)$$

which when solved for R yields

$$R = \frac{P \cos \theta}{2 \Sigma} \left[1 - \left(1 - \frac{4 A \Sigma}{P^2 \cos^2 \theta} \right)^{1/2} \right], \quad (13)$$

where P and A are the total perimeter and area of the container cross-section, respectively, and

$$\Sigma = \sum_{j=1}^n F_{Anj}$$

with F_{Anj} given by eq. (6). For the rhombic section of Fig. 2 is $\Sigma = 2F_{An}$. F_{Anj} is the dimensionless geometric constant of proportionality for the cross-flow area A_j and mean radius of curvature squared; namely,

$$A_j = R^2 F_{Anj} = f_j^2 h_j^2 F_{Anj}.$$

Note that Σ of eq. (13) bears no relation to Σ_i of eq. (11).

Modified Approach to Calculate R

An alternative application of the technique of de Lazzer et al may be pursued by identifying and analyzing symmetric sub-sections of a given container cross-section. For example, the smallest symmetric subsection of the rhombic cylinder example of Fig. 2 is the quarter section identified by dashed lines in Fig. 2b. This symmetric subsection is redrawn in Fig. 3. An additional angle θ_3 must be specified along the symmetry boundaries. Assuming the Concus-Finn condition is satisfied only at the acute vertex, eq. (11) for the geometry of Fig. 3 becomes

$$|\Sigma_1| \cos \theta_1 + |\Sigma_2| \cos \theta_2 + |\Sigma_3| \cos \theta_3 = |\Omega^*|/R. \quad (14)$$

Along the exposed (unwetted) faces of the rhombus Σ_1 , $\theta_1 = \theta$, the contact angle of the liquid on the wall material. Along the fluid interface spanning the corner Σ_2 , $\theta_2 = 0$. Additionally, because the dashed lines identify planes of symmetry for the surface, along Σ_3 , $\theta_3 = \pi/2$. Substitution of these quantities into eq. (14) produces

$$|\Sigma_1| \cos \theta + |\Sigma_2| = |\Omega^*|/R, \quad (15)$$

which is identical to eq. (12) only Σ_1 in this case does not include the symmetry plane portions of the perimeter of the subsection. Solving eq. (15) for R in this case yields

$$R = \frac{P_w \cos \theta}{2 \Sigma} \left[1 - \left(1 - \frac{4 A \Sigma}{P_w^2 \cos^2 \theta} \right)^{1/2} \right], \quad (16)$$

which produces the same value for R as computed by eq. (13) since for this symmetric subsection $\Sigma = F_{An}/2$, and P_w and A are 25% the values for the full domain solution, eq. (13). P_w is the perimeter of the section minus the symmetry boundaries.

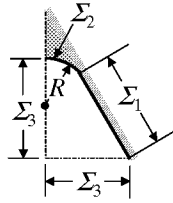


Fig. 3. Symmetric subsection for rhombus of Fig. 2. Symmetry planes identified by dashed lines.

As will be demonstrated, this modified approach to compute R is useful in determining flows in more complex containers. But the technique is fundamentally limited by the assumption of symmetric interfaces in symmetric containers. Uniqueness and stability of particular presumed interfacial configurations based on intuition and experience may also be difficult to establish¹⁰ and will depend on fluid fill level and history for real systems.

Calculation of R in Complex Cylindrical Containers with Symmetry

Cylindrical Tank with Central Radial Vanes

By viewing more complex container cross-sections as collections of symmetric subsections it is possible to compute R analytically for a variety of important container types with applications to low-g propellant/cryogen management.

For example, a cross-section of a long, partially-filled, right circular cylindrical propellant tank model with central radial vane structure is sketched in Fig. 4a. Again, due to the symmetry of the tank the equilibrium mean radius of curvature of the interface R may be determined by analyzing the smallest symmetrical element of the section as sketched in Fig. 4b. Assuming the Concus-Finn condition is satisfied between each of the vanes, eq. (16) for the geometry of Fig. 4b yields again

$$R = \frac{P_w \cos \theta}{2 \Sigma} \left[1 - \left(1 - \frac{4 A \Sigma}{P_w^2 \cos^2 \theta} \right)^{1/2} \right], \quad (17)$$

where $P_w = 2V + 2\alpha r$, $A = \alpha r^2$, and $\Sigma = F_{An}$ as given by eq. (6) for the wetted corner formed by the vane of vertex angle 2α . For $\theta = 0$, defining

nondimensional quantities $\mathcal{R} \equiv R/r$ and $\mathcal{V} \equiv V/r$, eq. (17) becomes

$$\mathcal{R} = \frac{(\mathcal{V} + \alpha)}{F_{An}} \left[1 - \left(1 - \frac{\alpha F_{An}}{(\mathcal{V} + \alpha)^2} \right)^{1/2} \right]. \quad (18)$$

Eq. (18) is constrained by at least the condition $\mathcal{R} \leq \mathcal{V} \sin \alpha / \sin \delta$; the interface cannot pin on the vane edges. Other constraints are possible, such as the case of wetting between the vanes and the circular tank wall which is not considered here though increasingly likely as the vane length \mathcal{V} approaches 1.

The symmetrical tank sketched in Fig. 4 may be generalized to a tank possessing n -vanes. For such a tank, and for $\theta = 0$, eq. (18) is presented in Fig. 5 for a variety of dimensionless vane lengths \mathcal{V} . The domain of each curve is limited by the constraint of no pinning on the vane edges. As is observed from the figure, the case of only 2 vanes with $\mathcal{V} = 0$ recovers the correct solution of the right circular cylinder without vanes, $\mathcal{R} = 0.5$. It is also observed from the figure how \mathcal{R} decreases with increasing number of vanes (decreasing α).

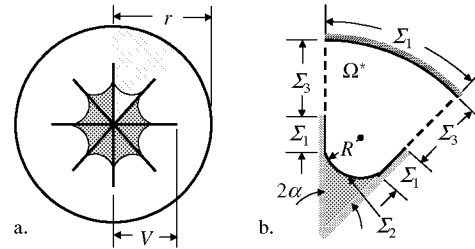


Figure 4. Simplified cylindrical tank model with central radial vane PMD: a. cross-section identifying wetted vanes, b. symmetric element of shaded region in a. with Σ_3 identifying symmetry planes.

Despite the limitation of no pinning allowed on the vane edge, the dimensional mean radius of curvature of the interface $R = r\mathcal{R}$ may be computed from eq. (18) for a number of vane lengths $V = r\mathcal{V}$ of practical importance.

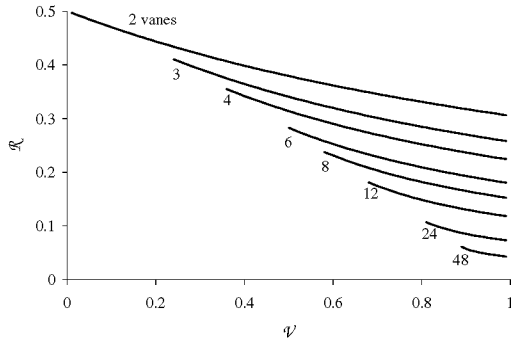


Figure 5. \mathcal{R} vs. Ψ for n -vaned tank patterned after the tank of Fig. 4.

Regular n -gon Tanks with Radial Wall Vanes

Another benchmark tank model readily addressed by the analysis outlined herein is that of regular polygonal cylindrical tanks with radial vanes emanating from the corner vertices. Several such tanks are sketched in Fig. 6 for $n = 3, 4, 6$, and 12 . As n increases this tank model approaches that of a right circular cylindrical tank with radial vanes emanating from the tank wall. The tank with $n = 12$ is presented in Fig. 7 in greater detail.

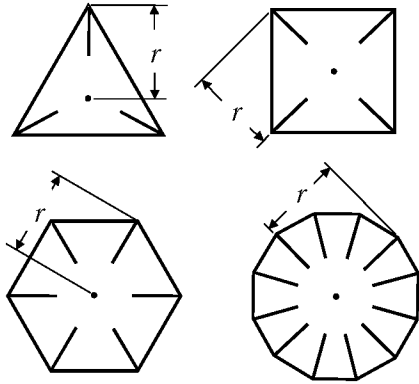


Figure 6. Regular polygonal tanks with radial wall vanes: $n = 3, 4, 6$, and 12 .

Again, due to the symmetry of the tank the mean radius of curvature of the interface R may be determined by analyzing the smallest symmetrical element of the section as sketched in Fig. 7b for the case $n = 12$. This element is a right triangle with acute vertex angles π/n and $\pi(1/2 - 1/n)$. Assuming $\theta = 0$, the Concus-Finn condition is satisfied in each interior corner formed by the vanes, and eq. (17) for this problem may be solved for R and nondimensionalized by tank circumscribing radius r yielding

$$\mathcal{R} = \frac{(\Psi + \sin(\pi/n))}{2 F_{An}} \left[1 - \left(1 - \frac{F_{An} \sin(2\pi/n)}{(\Psi + \sin(\pi/n))^2} \right)^{1/2} \right]. \quad (19)$$

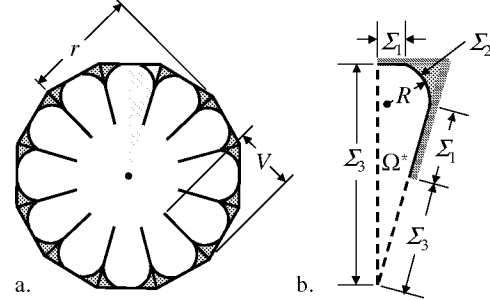


Figure 7. Regular polygonal tank with radial wall vanes, $n = 12$: a. cross-section identifying wetted vanes, b. symmetric element of shaded region in a. with Σ_3 identifying symmetry planes.

Eq. (19) is constrained by at least 2 conditions:

1. $\mathcal{R} \leq \Psi \sin \alpha / \sin \delta$, interfaces can not pin on vane edges.
2. $\mathcal{R} \leq \sin(\pi/n) \sin \alpha / \sin \delta$, a single interface can not span two corners.

Again, other constraints are possible, such as the case of a single interface wetting two vanes near the tank axis for large Ψ . This case is not considered here though increasingly likely as the vane length Ψ approaches 1.

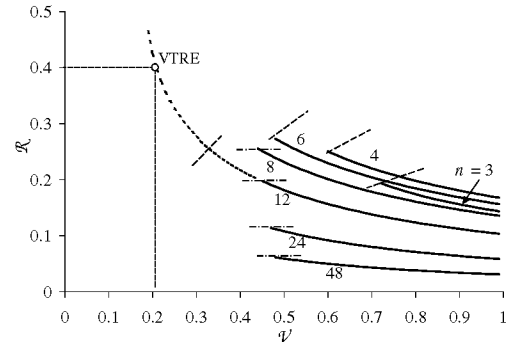


Figure 8. \mathcal{R} vs. Ψ from eq. (19) for tank of Figs. 6 and 7 with $n = 3, 4, 6, 8, 12, 24$, and 48 . Dashed line at curve terminus implies vane pinning constraint, dot-dashed line implies single interface spans two corners.

\mathcal{R} is computed via eq. (19) as a function of Ψ for a variety of n and presented in Fig. 8. The domain of the solutions is limited by at least the two constraints identified on the figure. For the

case $n = 12$, the curve identifying the complete range of $\mathcal{R}(\mathcal{V})$ with noted constraints is presented for later discussion.

Solution to Transient Flows using \mathcal{R}

Once \mathcal{R} is known for the tank, H_j values for each corner flow are computed using eq. (9) and the design quantities provided in eqs. (4), (5), and (6) may be determined. In addition, the entire surface profile of the liquid throughout the container may be computed. The solution follows from a global similarity solution and is applicable at long times throughout the container, despite the fact that both the flow and interface shape are not known in the neighborhood of the bulk meniscus². By approximating the global similarity solution for the meniscus centerline height in each corner by the polynomial

$$h_j \approx H_j(1 - 0.571\eta_j^+ - 0.429\eta_j^{+2}) \quad (20)$$

with

$$\eta_j^+ = 0.587 \left(\frac{\mu f_j}{\sigma H_j (F_i)_j \sin^2 \alpha_j} \right)^{1/2} z t^{-1/2} \quad (21)$$

subject to the constraint

$$\frac{\bar{\eta}_b^+ f_j}{F_{ij}^{1/2} \sin \alpha_j} \leq \eta_j^+ \leq 1$$

the 3-D transient interface in each corner may be computed via eq. (2).

Note that for the tanks of Figs. 4 and 7, the index j is somewhat superfluous since all interior corners of the tank are identical.

Examples of Design Utility

Cylindrical tanks may be designed with optimal characteristics using the analytical solution approach. A hypothetical example might be a PMD which would minimize tank rewetting time following resettling without an excessive mass penalty for unnecessary vanes. To address this optimization problem one might compute a ratio of total flow rate to total vane length. For the specific case of the central radial vane tank model sketched in Fig. 4 this ratio employs eq. (5) and is given by

$$\frac{n \dot{Q}_{tot}}{nV} = 0.349 \frac{F_{An}}{V} \left(\frac{\sigma F_i R^5 \sin^2 \alpha}{\mu f^2 t} \right)^{1/2}, \quad (22)$$

where V is the vane length and F_{An} , R , α , and f are functions of the number of vanes n . Substituting \mathcal{R} from eq. (18) into (22) and retaining only dimensionless geometrically-dependent terms, one computes

$$Q \equiv \frac{100 \sin \alpha}{f F_{An}^{3/2} \mathcal{V}} \left\{ (\mathcal{V} + \alpha) \left[1 - \left(1 - \frac{\alpha F_{An}}{(\mathcal{V} + \alpha)^2} \right)^{1/2} \right] \right\}^{5/2} \quad (23)$$

where the prefactor of 100 serves to make Q an $O(1)$ quantity for simplicity in presentation. For the tank with PMD sketched in Fig. 4, for $\theta = 0$, Q from eq. (23) is presented for a variety of vane lengths \mathcal{V} in Fig. 9. The vane edge pinning constraint restricts the range of each curve in a similar fashion as the curves computed and presented in Fig. 5. Q is maximized for $n = 12$, $\mathcal{V} = 0.68$, which means that the highest rewetting flow rate per unit vane length is achieved for these conditions for this PMD-type. (It is interesting to note that Q is maximized for $n = 12$ and thus $\alpha = 15^\circ$. This value also corresponds to the wedge half-angle yielding the maximum capillary flow rate for a fixed volume spreading drop¹¹.)

This example optimization is one of several that may be constructed for a variety of complex tank geometries. Such analytical schemes are quickly accomplished, accurate, and trivial in terms of commitment compared to numerically based techniques.

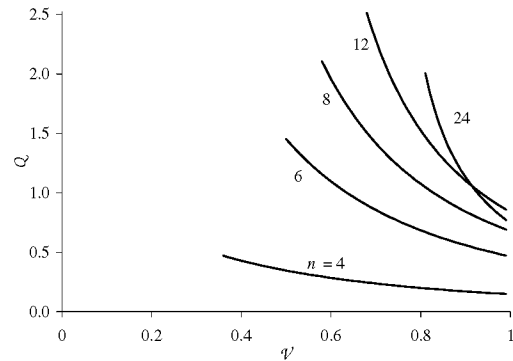


Figure 9. Dimensionless flow rate to vane length ratio Q for radial center vane PMD sketched in Fig. 3.

Limitations of the Theoretical Approach

The preceding analysis to compute R assumes a priori knowledge of the interior corners of the container that satisfy the Concus-Finn condition. The analysis also assumes knowledge of a local and symmetric equilibrium surface (one of perhaps many¹⁰). For more complex symmetric containers such as those shown in Figs. 4 and 7 it is assumed that the interface is also symmetric.

For the ensuing transient flow problem, the bulk interface is assumed to rapidly achieve a constant mean radius of curvature R . The interior corners must be sufficiently planar such that the flow may be approximated by the system defined by eq. (1), Fig. 1. The planar interior corners must also be of sufficient size such that the interface does not pin on wettability boundaries, i.e. the terminus of a vane (where the equilibrium contact angle is no longer unique). Such pinning flows are address analytically by Romero and Yost¹² and experimentally by Mann et al.¹³ Slightly non-planar interior ‘corners’ may be treated by a modified analytical approach¹⁴.

For cylindrical containers of increasing complexity, a generally increasing number of constraints must be applied to the solution for R . These constraints limit the range of applicability of the present solution procedure. Modified or alternate techniques may be developed for constraint conditions such as edge pinning or single interfaces spanning more than one interior corner. The more general though complex approach of Finn and Neel⁹ may also be applied. Such techniques will be discussed in a subsequent publication as will be the significant impact of contact angle hysteresis for real systems where $\theta > 0$, which has been ignored.

Application to Tank PMD Rewetting

The analysis outlined herein naturally applies to spontaneous capillary driven flow as occurs in liquid propellant tanks following termination of thruster firing for orbital maneuvering, docking, or tank resettling. Other examples include myriad low-g fluids management applications (i.e. on-orbit container filling) and drop tower tests. Attention here is focused on the former where the results of the Vented Tank Resupply Experiment (VTRE) provide in-flight data of PMD rewetting following thrust resettling.

VTRE PMD Rewetting after Thrust Resettling

VTRE was conducted aboard the Space Shuttle in 1996¹⁵. The experiment explored a variety of practical issues concerning propellant management in a space-based system. One of the tests performed involved thrust resettling of a 20% filled spherical tank with PMD: 12 axial radial (center post) vanes and 12 axial radial wall vanes. The test was conducted by exploiting the Orbiter primary Reaction Control (RCS) jets to settle the liquid contents in a most unfavorable location within the tank to observe the spontaneous redistribution of the liquid upon termination of the thrust. A schematic of the $r = 0.178\text{m}$ tank is provided in Fig. 10a with a cross-section in Fig. 10b. The test fluid was R-113 at 20 °C with $\sigma = 0.0167\text{N/m}$, $\mu = 7.21 \cdot 10^{-4} \text{ kg/m-s}$, $\rho = 1570 \text{ kg/m}^3$, and $\theta = 0$.

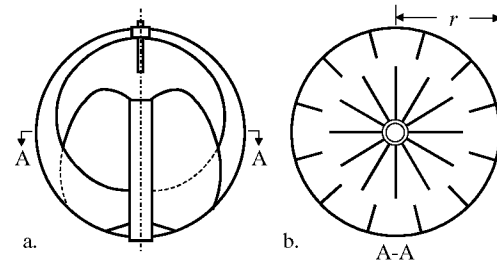


Figure 10. Spherical VTRE tank with 12 inner and outer radial vane PMD: $r = 0.1778 \text{ m}$. Tank vent at top, propellant outlet at bottom.

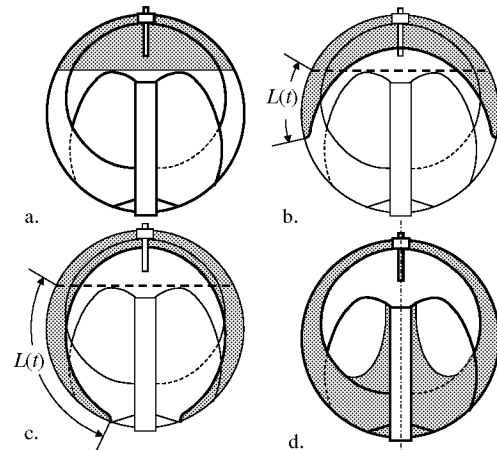


Figure 11. Approximate VTRE interface configurations for $\approx 20\%$ fill: a. effective equilibrium with $g > 7(10)^{-4}g_o$ ($g_o = 9.8\text{m/s}^2$) acting positive-upward, $t = 0$, b. $L(t)$ during PMD rewetting with $g \approx O(10^{-6}g_o)$, c. $L(t)$ at data termination, $g \approx O(10^{-6}g_o)$, $t = t_f$, d. equilibrium, $g \approx O(10^{-6}g_o)$.

The equilibrium interface for $g \approx 0$ is shown in Fig. 11d—liquid centered over propellant outlet, vapor centered over tank vent. During unfavorable thruster firing the liquid contents reorients to the configuration sketched in Fig. 11a. Following termination of the thruster firing the fluid spontaneously returns to the low- g equilibrium configuration of Fig. 11d by the combined influence of surface tension, surface wettability, and container/vane geometry. It is of critical design importance to understand quantitatively what minimal PMD will produce the desired performance.

As a first application of the theoretical technique to model PMD rewetting following termination of thruster firing, the VTRE data was re-analyzed to determine the transient meniscus tip location $L_f(t)$ in the interior corners of the tank formed by the vanes of the PMD. The fact that the tank was filled to approximately 20% led to the initial condition of a predominantly flat surface (Fig. 11a) that *did not* contact the center radial vane structure. Thus, upon termination of the thrust, rewetting of the tank consisted first of spontaneous corner flows along the radial wall vanes to the base of the central radial vane structure at the propellant exit port, Figs. 11b and 11c. The central radial vane structure was then wetted from below and the spontaneous flow along this path eventually returned the liquid to the equilibrium configuration shown in Fig. 11d.

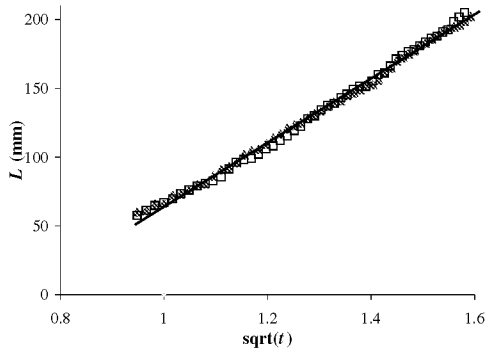


Figure 12. Corner tip location L vs. $t^{1/2}$ for VTRE during spontaneous rewetting of two outer wall vanes. Solid line is eq. (4) with $\mathcal{R} = \mathcal{R}_{VTRE} = 0.412$.

The flows of interest are identified schematically in Figs. 11b and 11c. VTRE data for the meniscus tip location L of two radial wall vanes is provided in Fig. 12. Significant optical distortions prevented accurate measurements for other vanes. These data are collected from the

VTRE flight video tapes following termination of the Orbiter RCS firing. The Tracker Image Analysis System developed by NASA¹⁶ is used to digitize the video images. The meniscus location is computed by applying optical corrections for camera rotation, depth of field, and projection of the 3-D spherical flow onto the 2-D CCD array. Measurement accuracy is estimated to be better than $\pm 5\%$, the largest uncertainty arising from a 5% change in scale factor from the front to midplane of the spherical tank. A tank flange obscured data for time less than that shown on Fig. 12.

For the two vanes analyzed, $L(t)$ is presented against $t^{1/2}$ in Fig. 12 as suggested by theory, eq. (4). The flows are nearly identical reflecting the degree of symmetry of the initial condition (thrust well-aligned with tank axis) and computed slopes for each vane agree to within 4%. Because the time for the initial wall rewetting was so short (< 1.7 s), L vs. t also appears linear for this test. Nonetheless, the precision of the linear fit for L vs. $t^{1/2}$ argues favorably for application of the transient analysis outlined herein. Thus, applying the form suggested by eq. (4) to the data of Fig. 12

$$L_{VTRE} = 0.232 t^{1/2}, \quad (24)$$

where the experimentally determined coefficient $0.232\text{m/s}^{1/2}$ is accurate to $\pm 5\%$. Increased uncertainty is expected for $t < 1$ s. It is insightful to mention that for this 0.356m diameter tank average corner flow velocities are as high as 0.232m/s within 1s of thrust termination. Such velocities increase with container size to the $1/2$ -power. Initial velocities in a similar 1m spherical tank and fluid are likely to be 0.39m/s.

Substituting the thermophysical properties of R-113, eq. (4) is equated to eq. (24) and solved to determine $\mathcal{R}_{VTRE} = 0.412$. This is the experimentally determined value of \mathcal{R} which when used to predict meniscus tip location $L(t)$ during rewetting provides the collapse of the experimental data illustrated in Fig. 12 and prediction by eq. (4) to within $\pm 5\%$.

Generalized VTRE Model Section

Because flight data of PMD rewetting is extremely rare it is of value to apply the analytical approach of this paper to the VTRE

tank PMD rewetting test despite the fact that the spherical VTRE tank with PMD violates numerous assumptions:

1. The tank is spherical, *not cylindrical*, and 3-D curvature affects might be expected to be significant.
2. The widths of both central and wall radial vanes vary with axial location.
3. The mean radius of curvature R for equilibrium interfaces is a significant function of fill level.
4. The VTRE tank might be considered ‘large’ and the rapid formation of a bulk interface with constant R seems unlikely.
5. VTRE experimental data show that the rewetting flows along the corners formed by the radial wall (outer) vanes eventually pin on the vane edges and that single interfaces are observed to span two interior corners formed by the outer wall vanes. It is noted that both occur near the end of the rewetting event.

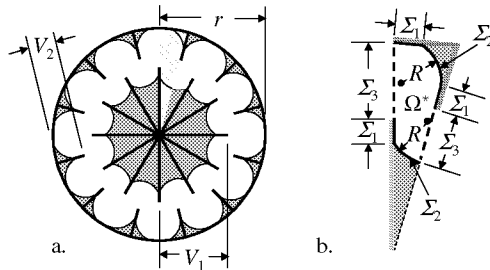


Figure 13. VTRE cylindrical tank model: a. cross-section identifying inner/outer wetted vanes, b. symmetric element of shaded region in a. with Σ_3 identifying symmetry planes.

In the face of such seeming complications the analytical technique is applied to model the VTRE PMD rewetting event. A generic cylindrical model of VTRE is sketched in Fig. 13a. The smallest symmetrical element is depicted in Fig. 13b. Due to the large number of vanes, the curved portion of the section is approximated as a straight section in Fig. 13b, in a fashion after the tank model of Fig. 7 with $n = 12$. However, unlike the example of Fig. 7, the curvature of the tank is modeled with improved precision by approximating the smallest symmetrical element as an isosceles triangle, rather than a right triangle. This decision is mute for large n , since the difference in models is measured by $1/n$. Eq. (17) for the cross-section in Fig. 13b yields

$$\mathcal{R} = \frac{\mathcal{F}}{2\Sigma_v} \left[1 - \left(1 - \frac{2\Sigma_v \sin \alpha_1}{\mathcal{F}^2} \right)^{1/2} \right], \quad (25)$$

where

$$\mathcal{F} \equiv (2 \sin(\alpha_1/2) + \mathcal{V}_1 + \mathcal{V}_2) \cos 6^\circ,$$

$$\Sigma_v \equiv F_{An1}/2 + F_{An2},$$

and subscripts 1 and 2 denote inner and outer vanes, respectively. (Note that $\alpha_1 = \pi/12$.)

The presumed interfacial configuration of Fig. 13 leads to eq. (25) for the prediction of \mathcal{R} . However, other more preferred configurations may arise, several of which are anticipated as sketched in Fig. 14. One approach to determine the transient flow problem for each configuration is to first assume the configuration, compute \mathcal{R} for that configuration using eq. (16), and apply the transient solutions of eqs. (4)-(6). The surface energy of a given interface configuration will help identify preferred states, but mathematical proof is required to establish if a given configuration is indeed unique⁹.

Concerning the configurations of Fig. 14: Fig. 14a is the case under consideration. Cases 14b and 14c are the limiting cases of interface pinning on \mathcal{V}_1 and \mathcal{V}_2 , respectively. Case 14d is the limiting case of a single interface (I_2) wetting two adjacent out vanes, \mathcal{V}_2 . Case 14e is the limiting condition of \mathcal{V}_2 intersecting the interface (I_1) in \mathcal{V}_1 . The cases of 14f, 14g, and 14h are actually different configurations and not limiting cases of the sought configuration 14a. Case 14f is the condition where I_1 wets both \mathcal{V}_1 and \mathcal{V}_2 and cases 14g and 14h arise when a third interface I_3 is present: 14g when I_1 only wets \mathcal{V}_1 and 14h when I_1 wets both \mathcal{V}_1 and \mathcal{V}_2 . Other configurations might be considered. For brevity in the following discussion, the cases of 14f, 14g, and 14h will not be consider despite being increasingly probable as \mathcal{V}_1 and \mathcal{V}_2 approach 1. The notation I_1 , I_2 , and I_3 is used to identify interfaces in the inner and outer vanes and between \mathcal{V}_1 and the outer wall, respectively, as indicated in Fig. 14.

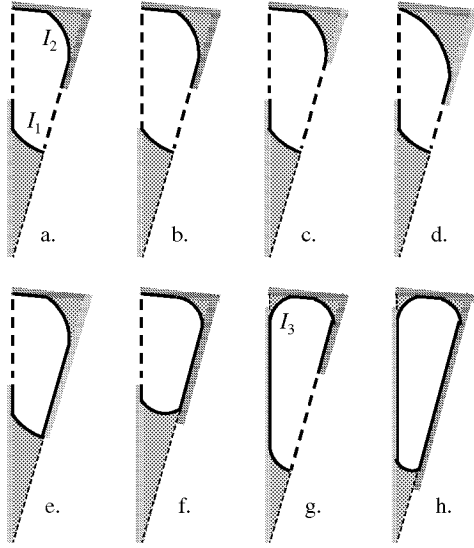


Fig. 14. Some possible interface configurations for the symmetric subsection of the VTRE model of Fig. 13.

The dimensionless mean radius of curvature $\mathcal{R}(\psi_1; \psi_2)$ from eq. (25) with $\theta = 0$ is presented in Fig. 15 for the range of possible ψ_2 values identified on the figure. For the interface configuration depicted in Fig. 13, the possible values for \mathcal{R} are at least constrained by:

1. $\psi_1 < 1$, ψ_1 may not contact tank wall.
2. $\psi_2 < 1$, ψ_2 may not contact center post.
3. $\mathcal{R} \leq \psi_1 \sin \alpha_1 / \cos \alpha_1$, I_1 does not pin on ψ_1 .
4. $\mathcal{R} \leq \psi_1 \tan(\pi/4 - \alpha_1/4)$, I_2 does not pin on ψ_2 .
5. $\mathcal{R} \leq f_1(1 - \psi_2)$, ψ_2 does not touch I_1 .
6. $\mathcal{R} \leq 2 \sin(\alpha_1/2) \tan(\pi/4 - \alpha_1/4)$, I_2 does not span 2 outer vane corners.
7. $\mathcal{R} \leq \mathcal{F}/2\Sigma_v$, \mathcal{R} cannot exceed tank maximum.

It is important to repeat that the above list is not exhaustive.

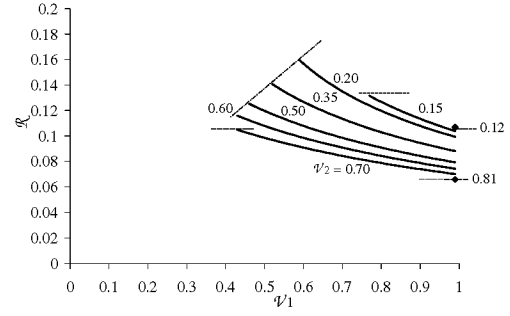


Figure 15. $\mathcal{R}(\psi_1; \psi_2)$ for tank sketched in Fig. 13. Upper horizontal dashed lines imply ψ_2 pinning, diagonal dot-dashed line implies ψ_1 pinning, lower horizontal dashed lines imply ψ_2 intersects I_1 .

VTRE Model Section: Special Case

For the special case of $\psi_2 = 0.35$, $\theta = 0$, eq. (25) is solved and presented in Fig. 15 along with constraints #3 through #7 identified for this VTRE-like cylindrical model. It is observed that the limiting constraint is interface pinning on the inner vanes (I_1 pins on ψ_1 , #3) and the curve for larger values of \mathcal{R} (smaller ψ_1) is approximate at best. Constraints #5 and #6 are coincidentally nearly identical for this special case of ψ_2 and the curve for lower values of ψ_1 is irrelevant since the fluid configuration is no longer even closely modeled by the schematic in Fig. 13.

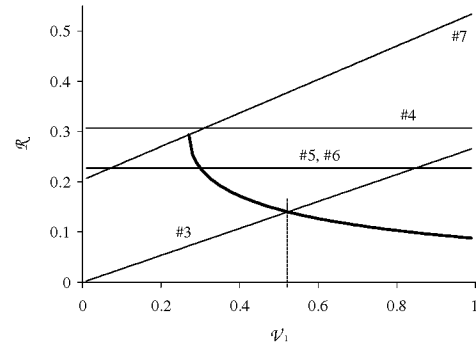


Figure 16. \mathcal{R} for model VTRE tank (Fig. 12) with $\psi_2 = 0.35$: Constraints are identified by list number for this geometry.

For the further restricted case of $\mathcal{V}_1 = 0.6$ and $\mathcal{V}_2 = 0.35$, the *Surface Evolver*⁴ algorithm is used to compute the full 3-D surface for a cylindrical tank of radius r , diameter D , and cylindrical section length L . The cylindrical tank has circular disc end caps (lids). The aspect ratio m of the cylindrical portion of the tank is defined by L/D . The computed equilibrium surface is shown in Fig. 17 for $\theta = 8.11^\circ$ for a tank with aspect ratio $m = 3$, and 52% liquid fill volume. A computed cross-section of the smallest symmetrical element at the mid-plane of the tank is shown in Fig. 18.

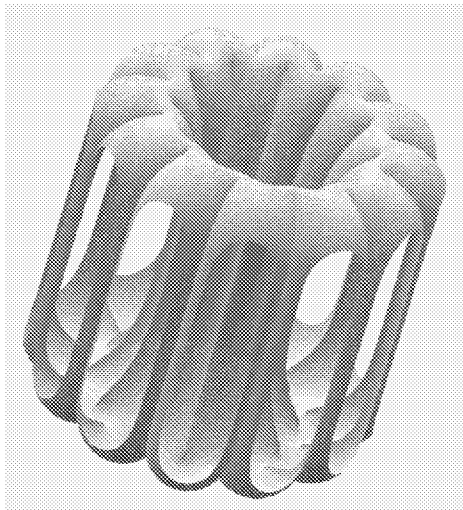


Figure 17. *Surface Evolver* solution of VTRE-like cylindrical model with $\mathcal{V}_1 = 0.6$, $\mathcal{V}_2 = 0.35$, $\theta = 8.11^\circ$. Oval voids on the perimeter are dry region of the tank wall.

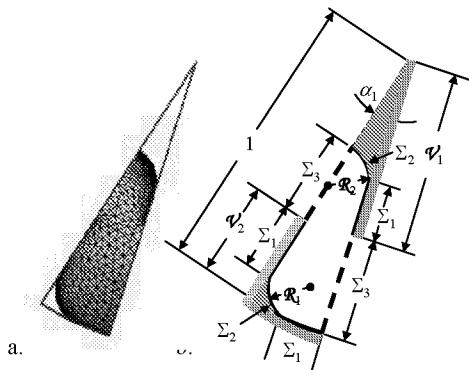


Figure 18. Smallest symmetrical element cross-section of cylindrical VTRE model shown in Fig. 17: a. *Surface Evolver* solution, b. schematic identifying parameters. Compare with Fig. 13b.

Several *Surface Evolver*-computed values (*SE*) for the container mean radius of curvature \mathcal{R} are listed in Tables 1 through 4 for comparison with values computed using eq. (25). Holding all other parameters fixed, Tables 1-4 list values for \mathcal{R} dependent on contact angle θ , vane lengths \mathcal{V}_1 and \mathcal{V}_2 , aspect ratio m , and liquid fill level. Nominal uncertainties for the *SE* results are provided. The two techniques to determine \mathcal{R} are in excellent agreement.

Local *SE*-computed values for \mathcal{R}_1 and \mathcal{R}_2 for the respective surfaces adjacent to \mathcal{V}_1 and \mathcal{V}_2 are also listed in the tables for each case. These radii are computed in the plane bisecting the container normal to the cylinder axis (Fig. 18). The differences between \mathcal{R} for the tank computed by eq. (25) and \mathcal{R}_1 and \mathcal{R}_2 computed by *SE* provide a measure of error for the use of eq. (25) arising from the infinite container assumption. This error might be considered small in light of such low aspect ratio m containers. It is clear from Table 2 that all *SE* values for \mathcal{R}_1 and \mathcal{R}_2 approach eq. (25) values for \mathcal{R} as m increases.

Table 1. Comparison of present theory eq. (25) and *Surface Evolver* (*SE*) computations: Effect of contact angle θ , $\mathcal{V}_1 = 0.6$, $\mathcal{V}_2 = 0.35$, $m = 1$, $Q_{liq} = 55\%$.

θ ($^\circ$)	\mathcal{R}_{theo} eq.(25)	\mathcal{R} <i>SE</i>	\mathcal{R}_1 <i>SE</i>	err. (%)	\mathcal{R}_2 <i>SE</i>	err. (%)
0	0.1268	0.1273	0.138	7.2	0.122	1.6
5	0.1271	0.1276	0.134	0.4	0.122	1.6
10	0.1279	0.1285	0.135	1.5	0.128	1.6
20	0.1319	0.1325	0.140	4.3	0.132	1.5
30	0.1399	0.1406	0.154	0.6	0.141	1.4
40	0.1540	0.1550	0.176	0.5	0.161	1.2
44.7	0.1639	0.1653	0.189	3.7	∞	-

Table 2. Results of *Surface Evolver*: Effect of aspect ratio m ; volume of liquid fixed, $\theta = 0$, $\mathcal{R}_{theo} = 0.1268$, $\mathcal{V}_1 = 0.6$, $\mathcal{V}_2 = 0.35$. Case $m = 2$ almost uncovers lid, case $m = 4$ uncovers lid.

m (L/D)	\mathcal{R} <i>SE</i>	\mathcal{R}_1 <i>SE</i>	err. (%)	\mathcal{R}_2 <i>SE</i>	err. (%)	Q (%)
0.75	0.1260	0.158	3.3	0.144	6.9	73
1	0.1273	0.138	7.2	0.122	1.6	55
2	0.1269	0.128	0.0	0.122	8.2	28
4	0.1059	0.107	0.4	0.103	9.7	14

Table 3. Results of *Surface Evolver*: Effect of liq. fill Q_{liq} ; $\theta = 0$, $R_{theo} = 0.1268$, $\mathcal{V}_1 = 0.6$, $\mathcal{V}_2 = 0.35$, $m = 1$.

Q_{liq} (%)	\mathcal{R} <i>SE</i>	\mathcal{R}_l <i>SE</i>	err. (%)	\mathcal{R}_c <i>SE</i>	err. (%)
30	0.1273	0.130	2.3	0.122	8.2
55	0.1273	0.138	7.2	0.122	1.6
70	0.1271	0.144	2.1	0.136	7.3
80	0.1260	0.160	1.2	0.153	6.5

Table 4. Results of *Surface Evolver*: Effect of vane size/ratio \mathcal{V}_1 , \mathcal{V}_2 ; $\theta = 20^\circ$, $m = 1$, $Q_{liq} = 55\%$, *SE* errors $< 2\%$.

\mathcal{V}_1	\mathcal{V}_2	R_{theo} eq. (25)	\mathcal{R} <i>SE</i>	\mathcal{R}_l <i>SE</i>	\mathcal{R}_c <i>SE</i>
0.60	0.35	0.1268	0.1325	0.140	0.132
0.60	0.45	0.1134	0.1193	0.131	0.125
0.90	0.35	0.1031	0.1001	0.103	0.100

Comparison of Theory and Experiment: VTRE

As previously mentioned, the VTRE rewetting event only involved the outer radial wall vanes due to a low fill level in the spherical tank as depicted in Fig. 11. Thus the cylindrical tank geometry discussed in this paper that models the spherical VTRE tank rewetting event following thrust resettling is that of Fig. 7. \mathcal{R} for this cylindrical model was solved as a function of \mathcal{V} and presented in Fig. 8.

By equating radii of the spherical VTRE tank and cylindrical VTRE model, and by evaluating \mathcal{V} based on initial interface location (refer Fig. 11a) and detailed VTRE design drawings¹⁷ represented only schematically in Fig. 10, a value of $\mathcal{V} = 0.21$ may be determined for the rewetting event. As demonstrated in Fig. 8, with $n = 12$, this low value for \mathcal{V} shows that, at equilibrium, the interface pins on the vane edges and single interfaces cover two interior corners formed by adjacent vanes. Thus, both constraints #1 and #2 are violated. Nonetheless, observations of the flight video show that such constraints are not exceeded during the larger portion of the transient event. If these constraints were ignored for the transient rewetting one might simply use the value of \mathcal{R} computed from eq. (19) with $n = 12$ and $\mathcal{V} = 0.21$. As shown using dashed lines in Fig. 8, $\mathcal{R} = 0.396$ computed in this manner, which is in surprisingly favorable agreement ($< 4\%$)

with $\mathcal{R}_{VTRE} = 0.412$ determined experimentally. An even better prediction is possible using eq. (25) setting $\mathcal{V}_1 = 0$, $F_{An1} = 0$, with $\mathcal{V}_2 = 0.21$. For this case $\mathcal{R} = 0.419$. This value is within $< 2\%$ of \mathcal{R}_{VTRE} , the improvement arising from the approximation of the symmetric subsection as an isosceles triangle as opposed to a right triangle. Both predictions, using eqs. (19) or (25), are correct to within the experimental uncertainty of 5% for $\mathcal{V}_2 = 0.21$.

Table 5. Predicted and measured \mathcal{R} for VTRE.

Technique	\mathcal{R}
Predicted, eq. (19)	0.396
Predicted, eq. (25)	0.419
Measured eq. (24), Fig. 12	0.412

Further Considerations

Following an acceptable agreement for \mathcal{R} between theoretical predictions and VTRE flight results compared in Table 5, the theoretical approach, which allows the closed form calculation of the most important flow characteristics such as rise height and flow rate, can be used to compute transient interface shapes throughout the container. For example, the surface within the smallest symmetric sub-section of the cylindrical 24 vane VTRE model (Fig. 13) is computed in Fig. 19 at various times. The tip rise height and receding bulk meniscus location may be determined explicitly by eqs. (4) and (6), respectively. The latter is exaggerated by a factor of 2 in Fig. 19 to clearly illustrate the ‘draining’ of the container by the corner flows.

The full VTRE model is computed and shown in Fig. 20 at time $t = 2.5s$ —the approximate duration of the initial VTRE PMD rewetting event had all the vanes been wetted. The VTRE model with only exterior vanes wetted is also computed and shown in Fig. 21 at time $t = 2.5s$ —the model of the PMD rewetting process actually achieved on-orbit. (Note that \mathcal{R} in Fig 21 without the central vanes is significantly larger than \mathcal{R} in Fig. 20 with the central vanes.) Computations of such surfaces serve well to illustrate the wealth of information contained within the closed form analytic solutions reported herein.

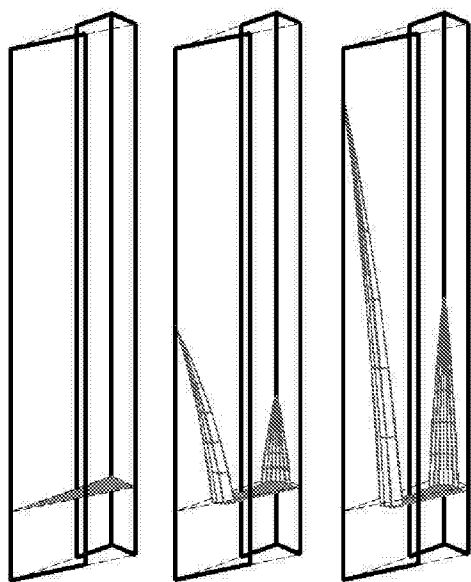


Fig. 19 Transient corner flows in smallest symmetrical sub-section of 24-vane VTRE model (times $t = 0, 0.5, 1.0, 1.5, 2.5$).

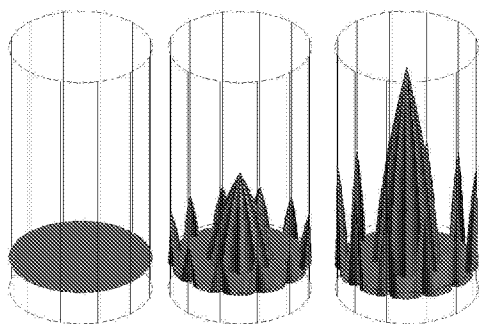


Fig. 20. Full VTRE model surface at $t = 0, 0.5, 2.5$ s. 12 Inner and 12 outer vanes not shown.

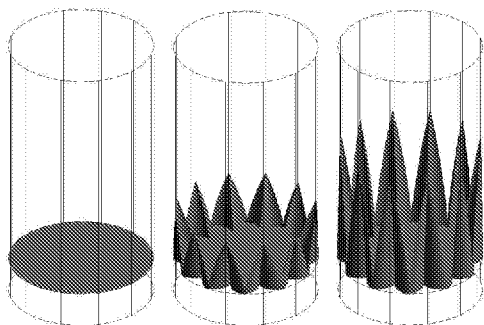


Fig. 21. VTRE model surface without central vanes at $t = 0, 0.5, 2.5$ s. Model approximates flight condition of PMD rewetting after thrust resettling. 12 outer vanes not shown.

Concluding Remarks

The literature reports an accurate analytical solution approach to predict spontaneous capillary flows in containers with interior corners. Such flows are important to a variety of low-g fluids handling operations including propellant management. In this paper a procedure is outlined and demonstrated that culminates in the prediction of transient flows in complex cylindrical containers that are symmetric, or where the contact angles θ_i around the projected cross-section may be specified. The general steps are:

1. Identify the interior corners of the tank satisfying the Concus-Finn wetting condition.
2. Derive the mean radius of interfacial curvature \mathcal{R} for the tank.
3. Identify and derive the constraints on \mathcal{R} .
4. Compute H_j from \mathcal{R} for each wetting corner of the tank and compute important transient quantities such as flow distance, flow rate, receding meniscus location and entire surface shape.

In this paper the important unknown quantity is \mathcal{R} , the dimensionless mean radius of curvature of the interface at equilibrium, knowledge of which enables the determination of the correct initial condition for the sought transient solutions. The theory of de Lazzar et al³ to compute \mathcal{R} is modified to account for symmetry planes within complex cylindrical tanks. Three cylindrical vanned tank-types of increasing complexity are modeled to demonstrate the approach to compute \mathcal{R} : a circular tank with central radial vanes (Fig. 4), a tank with wall mounted radial vanes (Fig. 7), and a combination tank which serves as a model for the Vented Tank Resupply Experiment (VTRE) Shuttle flight tests (Fig. 13). It is shown that even for the most complex tank, agreement in \mathcal{R} for the present theory with 3-D numerical predictions is typically better than 5% for aspect ratio containers of about 1 or greater. The results apply in general to symmetrical polygonal tanks and certain tanks with curved walls as demonstrated. Some of the limitations of the theory are noted.

The results of the analysis greatly speed and simplify calculations of capillary driven flows in complex containers which model important problems such as PMD rewetting following thrust resettling. Experiments concerning PMD rewetting were conducted during VTRE testing and these data are digitized and presented in Fig. 12. \mathcal{R} computed from the VTRE experimental data agrees to $\pm 4\%$ with \mathcal{R} computed using the theoretical approach as shown in Table 5, despite the apparent violation of a significant number of assumptions.

The all-analytical approach espoused herein may be used to quickly and accurately determine solutions to problems commonly thought to require extensive 3-D transient CFD. The approach is ideal for design optimization and an example problem is solved. The technique may be applied as a guide to CFD modeling, or serve as a ‘benchmark’ to numerical techniques in certain limiting cases. The analytic approach may also be exploited to design test tanks mimicking the smallest symmetrical sub-section of larger tanks for ground tests (i.e. low-g aircraft). The tanks may be significantly smaller than the full-scale tanks, or even scale models, making data taken from brief periods of low-g more representative of on-orbit performance.

References

- ¹M.M. Weislogel, S. Lichter, Capillary Flow in Interior Corners, *J. Fluid Mech.*, **373**:349–378, Nov. 1998.
- ²M.M. Weislogel, Capillary Flow in Containers of Polygonal Section, *AIAA J.*, **39**(12):320–2326, Dec. 2001.
- ³A. de Lazzer, D. Langbein, M. Dreyer, J. Rath, Mean curvature of liquid surfaces in containers of arbitrary cross-section, *Microgravity sci. technol.*, **IX**(3):208–219, 1996.
- ⁴K.A. Brakke, *Surface Evolver* program, the code and manual are available at <http://www.susqu.edu/facstaff/b/brakke/>.
- ⁵P. Concus; R. Finn, On the behavior of a capillary surface in a wedge, *Appl. Math. Sci.*, **63**(2), 292–299, 1969.
- ⁶M. Dong, I. Chatzis, The imbibition and flow of a wetting liquid along the corners of a square capillary tube, *J. Colloid and Int. Sci.*, **172**:278–288, 1995.
- ⁷D. Langbein, M.M. Weislogel, Dynamics of Liquids in Edges and Corners (DYLCO): IML–2 Experiment for the BDPU, NASA TM 1998-207916, Aug. 1998.
- ⁸D.E. Jaekle Jr., Propellant management device conceptual design and analysis: vanes, AIAA-SAE-ASME-ASEE 27th Jt. Propul. Conf., AIAA-91-2172, Sacramento, CA, June 1991.
- ⁹S.H. Collicott, private communication, Aug. 2002.
- ¹⁰R. Finn, R.W., Neel, C-Singular Solutions of the Capillary Problem, *J. reine angew. Math.* **512**, 1–25, 1999.
- ¹¹M.M. Weislogel, S. Lichter, A Spreading Drop in an Interior Corner: Theory and Experiment, *Microgravity Sci. Technol.*, **IX**(3):175–184, 1996.
- ¹²L.A. Romero, F.G. Yost, Flow in an Open Channel Capillary, *J. Fluid Mech.*, **322**, pp. 109–129, 1996.
- ¹³J.A. Mann, Jr., L. Romero, R.R. Rye, F.G. Yost, Flow of Simple Liquids Down Narrow V Grooves, *Physical Review E*, **52**:4, pp. 3967–3972, 1995.
- ¹⁴M.M. Weislogel, Capillary Flow in Interior Corners: the Infinite Corner, *Phys. of Fluids*, **13**(11):3101–3107, Nov. 2001.
- ¹⁵D.J. Chato, T.A. Martin, Vented Tank Resupply Experiment—Flight Test Results, 33rd AIAA-ASME-SAE-ASEE Int. Propulsion Conference, AIAA-97-2815 July 6–9, Seattle, 1997.
- ¹⁶R.B. Klimek, T.W. Wright, R.S. Sielken, Color Image Processing and Object Tracking System, NASA TM–107144, NASA Glenn Research Center, 1996.
- ¹⁷J. Gille, T. Martin, Vented Tank Resupply Experiment (VTRE), Final Technology Requirements Document, Martin Marietta MCR–91–1346, Contract NAS3–25977, Sept. 1993.

REPORT DOCUMENTATION PAGE			Form Approved OMB No. 0704-0188	
Public reporting burden for this collection of information is estimated to average 1 hour per response, including the time for reviewing instructions, searching existing data sources, gathering and maintaining the data needed, and completing and reviewing the collection of information. Send comments regarding this burden estimate or any other aspect of this collection of information, including suggestions for reducing this burden, to Washington Headquarters Services, Directorate for Information Operations and Reports, 1215 Jefferson Davis Highway, Suite 1204, Arlington, VA 22202-4302, and to the Office of Management and Budget, Paperwork Reduction Project (0704-0188), Washington, DC 20503.				
1. AGENCY USE ONLY (Leave blank)	2. REPORT DATE October 2002	3. REPORT TYPE AND DATES COVERED Final Contractor Report		
4. TITLE AND SUBTITLE Analysis of Tank PMD Rewetting Following Thrust Resettling		5. FUNDING NUMBERS WU-101-13-0B-00 NAS3-00126		
6. AUTHOR(S) M.M. Weislogel, M.A. Sala, and S.H. Collicott				
7. PERFORMING ORGANIZATION NAME(S) AND ADDRESS(ES) Portland State University P.O. Box 751 Portland, Oregon 97207-0751		8. PERFORMING ORGANIZATION REPORT NUMBER E-13618		
9. SPONSORING/MONITORING AGENCY NAME(S) AND ADDRESS(ES) National Aeronautics and Space Administration Washington, DC 20546-0001		10. SPONSORING/MONITORING AGENCY REPORT NUMBER NASA CR-2002-211974		
11. SUPPLEMENTARY NOTES M.M. Weislogel and M.A. Sala, Portland State University, P.O. Box 751, Portland, Oregon 97207-0751; and S.H. Collicott, Purdue University, West Lafayette, Indiana 47907-1968. Technical contact, Enrique Ramé, Microgravity Science Division, NASA Glenn Research Center, organization code 6712, 216-433-2842.				
12a. DISTRIBUTION/AVAILABILITY STATEMENT Unclassified - Unlimited Subject Categories: 34 and 20 Available electronically at http://gltrs.grc.nasa.gov This publication is available from the NASA Center for AeroSpace Information, 301-621-0390.			12b. DISTRIBUTION CODE	
13. ABSTRACT (Maximum 200 words) Recent investigations have successfully demonstrated closed-form analytical solutions of spontaneous capillary flows in idealized cylindrical containers with interior corners. In this report, the theory is extended and applied to complex containers modeling spacecraft fuel tanks employing propellant management devices (PMDs). The specific problem investigated is one of spontaneous rewetting of a typical partially filled liquid fuel/cryogen tank with PMD after thrust resettling. The transients of this flow impact the logistics of orbital maneuvers and potentially tank thermal control. The general procedure to compute the initial condition (mean radius of curvature for the interface) for the closed-form transient flows is first outlined then solved for several 'complex' cylindrical tanks exhibiting symmetry. The utility and limitations of the technique as a design tool are discussed in a summary, which also highlights comparisons with NASA flight data of a model propellant tank with PMD.				
14. SUBJECT TERMS Fuel tanks; Capillary flow; Corners; Liquid fuels; Propellants; Orbital maneuvers			15. NUMBER OF PAGES 21	
			16. PRICE CODE	
17. SECURITY CLASSIFICATION OF REPORT Unclassified	18. SECURITY CLASSIFICATION OF THIS PAGE Unclassified	19. SECURITY CLASSIFICATION OF ABSTRACT Unclassified	20. LIMITATION OF ABSTRACT	